3-D seismic images of large volumes of magma crystallized in the lower crust

T. Wrona[1,2]*, C. Magee[3,4], H. Fossen[5], R. L. Gawthorpe[1], R. E. Bell[3],
C. A-L. Jackson[3] & J. I. Faleide[6]

[1]Department of Earth Science, University of Bergen, Allgaten 41, N-5007 Bergen, Norway.
[2]Norwegian Academy of Science & Letters, Drammensveien 78, 0271 Oslo, Norway.
[3]Basins Research Group (BRG), Department of Earth Science and Engineering, Imperial College, Prince Consort Road, London, SW7 2BP, UK.
[4]School of Earth and Environment, University of Leeds, Leeds, LS2 9JT, UK
[5]Museum of Natural History, University of Bergen, Allgaten 41, N-5007 Bergen, Norway.
[6]Department of Geosciences, University of Oslo, P.O. Box 1047 Blindern, N-0316 Oslo, Norway.

*thilo.wrona@uib.no

Abstract

When continents rift, magmatism can produce large volumes of melt that migrate upwards from deep below the Earths surface. To understand the role of magmatism in rifting, it is critical to understand how much melt is generated and how it transits the crust. Estimating melt volumes and pathways is however difficult particularly in the lower crust where the resolution of geophysical techniques is limited. New broadband seismic reflection data allow us to image the 3-D geometry of magma crystallized in the lower crust (17.5-22 km depth) of the northern North Sea, in an area previously considered a magma-poor rift. The sub-horizontal magmatic intrusion is $\sim$97 km long (N-S), $\sim$62 km wide (E-W), and comprises several irregular lobes. The significant areal extent of the intrusion ($\sim$2700 km^2), as well as presence of intrusive steps indicate widespread lateral magma transport in the lower crust. We estimate that 472$\pm$161 km^3 of magma was emplaced within this intrusion, suggesting that the northern North Sea is more magmatic than previously thought.

Keywords: Magmatic intrusion, lower crust, 3-D seismic reflection data, North Sea

1 Introduction

The style of continental rifting critically depends on the strength of the lower crust (e.g. Huismans and Beaumont, 2011), which may be changed by magmatic processes, such as melting, magma migration and crystallization. To study the effects of magmatism on rifting, we need to understand the distribution, migration, and volume of magma emplaced in the crust in 3D (White et al., 2008). Whilst the current paradigm for magma plumbing system structure advocates that vertically stacked sills accumulate and store melt within the lower crust (e.g. Annen et al., 2005; Annen et al., 2015; Cashman et al., 2017; Edmonds et al., 2019), the lateral extent of these intrusion networks remains poorly understood. Three-dimensional seismic reflection data showing acoustic images of the subsurface have revolutionized our understanding of magma plumbing systems in the upper crust (e.g. Trude et al., 2003; Planke et al., 2005). In contrast, in the lower crust, seismic studies have long been limited by data coverage and resolution, providing an incomplete picture of the geometry and distribution of lower crustal intrusions (e.g. Cartwright and Hansen, 2006; Abdelmalak et al., 2017).

Using one of the largest 3-D seismic reflection surveys ever acquired (courtesy of CGG), covering 35,410 km^2 of the northern North Sea rift and imaging down to depths of 22 km, we are able to analyze lower crustal structures at a resolution of a few tens of meters over thousands of square kilometers. This allows us to critically examine and develop hypotheses for the origin of a lower crustal reflection (LCR), which has previously been identified in sparse 2-D seismic profiles (Christiansson et al., 2000; Fichler et al., 2011), but which we here are able to map in 3-D. Combining a series of detailed seismic (e.g. amplitude, polarity, continuity) and geometric observations (e.g. lobes, saucers, intrusive steps), we conclude that the LCR originates from an extensive, now-crystallized magmatic intrusion (±2700 km^2), which previously stored large volumes of magma (472±161 km^3) deep in the lower crust (17.5-22 km).
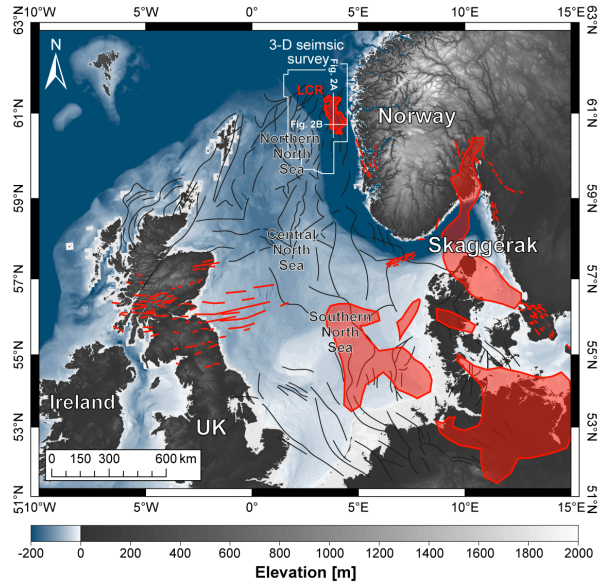
Figure 1: Location map of the North Sea showing the area covered by the 3-D seismic survey (courtesy of CGG) with LCR (white outline), magmatic dikes (red lines), tectonic faults (black lines) and volcanic rocks (red polygons) emplaced between the Late Carboniferous (∼300 Ma) and the Late Triassic (∼220 Ma) as part of the Skagerrak-centered Large Igneous Province (Fossen and Dunlap, 1999; Bingen and Solli, 2009; Fazlikhani et al., 2017). Offshore the distribution of volcanic rocks is constrained by well and seismic data (Heeremans and Faleide, 2004; Torsvik et al., 2008; Phillips et al., 2017). Topography and bathymetry are from ESRIs World Elevation Service (Weatherall et al., 2015).

2 Geological setting

The study area is located in the northern North Sea (Fig. 1), where continental crust consists of 10-30 km thick crystalline basement overlain by up to 12 km of sedimentary strata deposited during, after, and possibly even before periods of Late Permian-Early Triassic and Middle Jurassic-Early Cretaceous rifting (e.g. Bell et al., 2014; Maystrenko et al., 2017). The crystalline basement formed by terrain accretion during the Sveconorwegian (1140-900 Ma) and Caledonian (460-400 Ma) orogenies (Bingen et al., 2008). During the Caledonian Orogeny, subduction of continental crust subjected some of these basement rocks to high- and ultra-high

pressure conditions sufficient for partial eclogitization (Austrheim, 1987). A lower crustal reflection (LCR) identified in older 2-D seismic reflection data imaging our study area is characterized by a high-amplitude and positive polarity, and has previously been suggested to mark the top of a km-thick volume of eclogitized rocks (Christiansson et al., 2000). In contrast, Fichler et al. (2011) infer the LCR defines the boundary between overlying crystalline basement and an underlying, high magnetic susceptibility, serpentinized mantle wedge based on 2-D gravity and magnetic modelling. Testing these existing hypotheses for the origin of the LCR in the context of the geodynamic evolution of the northern North Sea using 3-D seismic reflection data is the focus of this study.
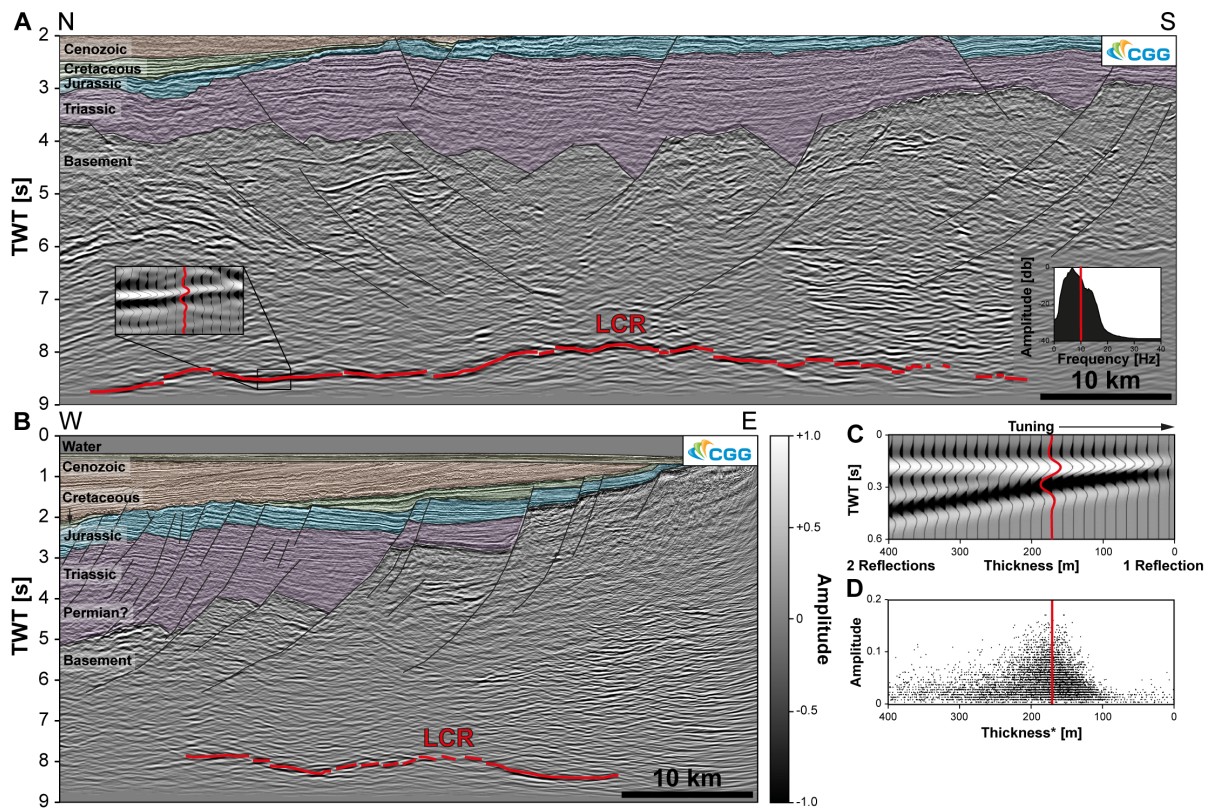
Figure 2: A: Seismic sections showing the lower crustal reflection (LCR) in N-S direction with zoom-in of seismic trace indicating peak-trough- wavelet similar to tuning wedge (**C**) and with frequency amplitude spectrum showing dominant frequencies of 10 ± 2 Hz around the LCR. **B:** Seismic section in E-W direction. **C:** Tuning wedge model based on acoustic impedance increase with depth. **D:** Thickness versus amplitude cross-plot of the LCR with thicknesses* calculated from the time difference between top and bottom reflection using an interval velocity of 6.9 km/s (Rosso, 2007). Note consistency of thickness estimates (180 ± 40 m) between **C** and **D**. Seismic data courtesy of CGG.

3   Observations

The LCR appears as a high-amplitude, positive polarity seismic reflection in the lower crust (17.5-22 km depth) (Figs. 2, 3; Supp. Fig. 1), and can be mapped continuously over ~2700 km^2 (Fig. 4, Supp. Fig. 2). The LCR comprises a ~97 km long (N-S) and ~62 km wide (E-W) surface consisting of several irregular lobes that laterally extend up to ~20 km outwards from its center (Fig. 3B, 4). These lobes themselves consist of several smaller, laterally connected saucer geometries (Figs. 3C; 4). These saucers are also the deepest part of the LCR, extending down to a depth of 22 km, whereas the central part of the LCR is much shallower (17.5 km).
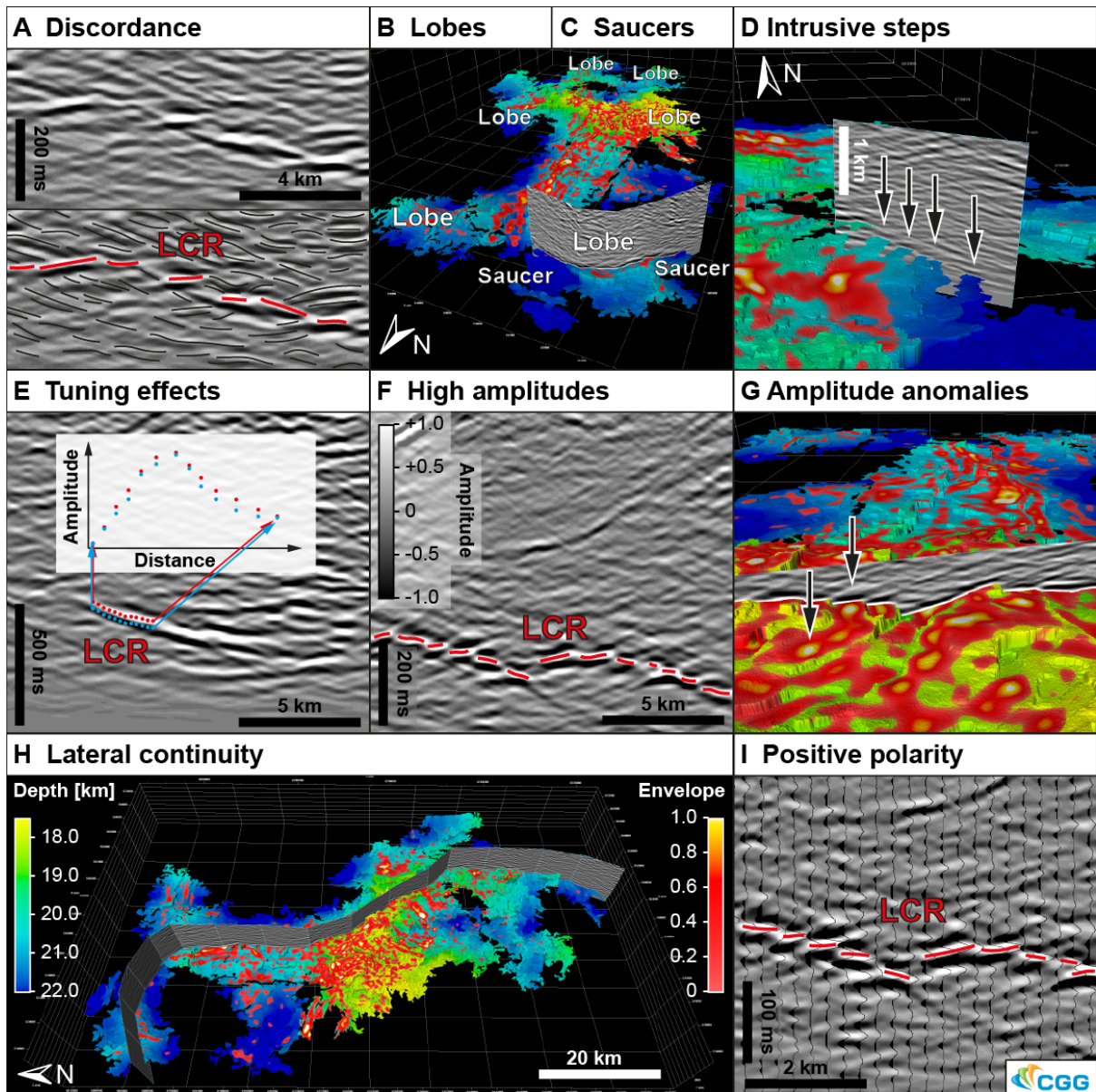
Figure 3: Seismic features of a magmatic intrusion observed on the LCR including: **A:** Discordance (e.g. Cartwright and Hansen, 2006; Magee et al., 2016), **B:** Lobe geometries (e.g. Smallwood and Maresh, 2002; Magee et al., 2016). **C:** Saucer geometries (e.g. Polteau et al., 2008; Keller et al., 2013; Infante-Paez and Marfurt, 2018). **D:** Intrusive steps (e.g. Hansen et al., 2004; Magee et al., 2016; McBride et al., 2018). **E:** Tuning effects, **F:** High amplitudes, **G:** Amplitude anomalies (e.g. Smallwood and Maresh, 2002). **H:** Lateral continuity (e.g. Magee et al., 2016), **I:** Positive polarity. Seismic data courtesy of CGG.

The center also displays a series of elongated, 100-300 m high vertical steps, which crosscut discontinuous, medium- to low-amplitude, background reflections (Figs. 3A, 4), as well as several elongate amplitude anomalies aligned along these steps in the horizontal plane (Figs. 3G, 4).

In general, the LCR shows: (1) high amplitudes, (2) a peak-trough wavelet, and (3) approximately equal peak and trough amplitudes, features that are typical of tuning effects (e.g. Widess, 1973; Robertson and Nogami, 1984; Sheriff and Geldart, 1995) (Figs. 2, 3E). Tuning occurs when seismic waves originating from the top and base of a thin body interfere on their return to the surface (e.g. Brown, 2011). We can estimate the thickness of a body where constructive interference from top and base produces a single tuned response, rather than two separate seismic reflections.
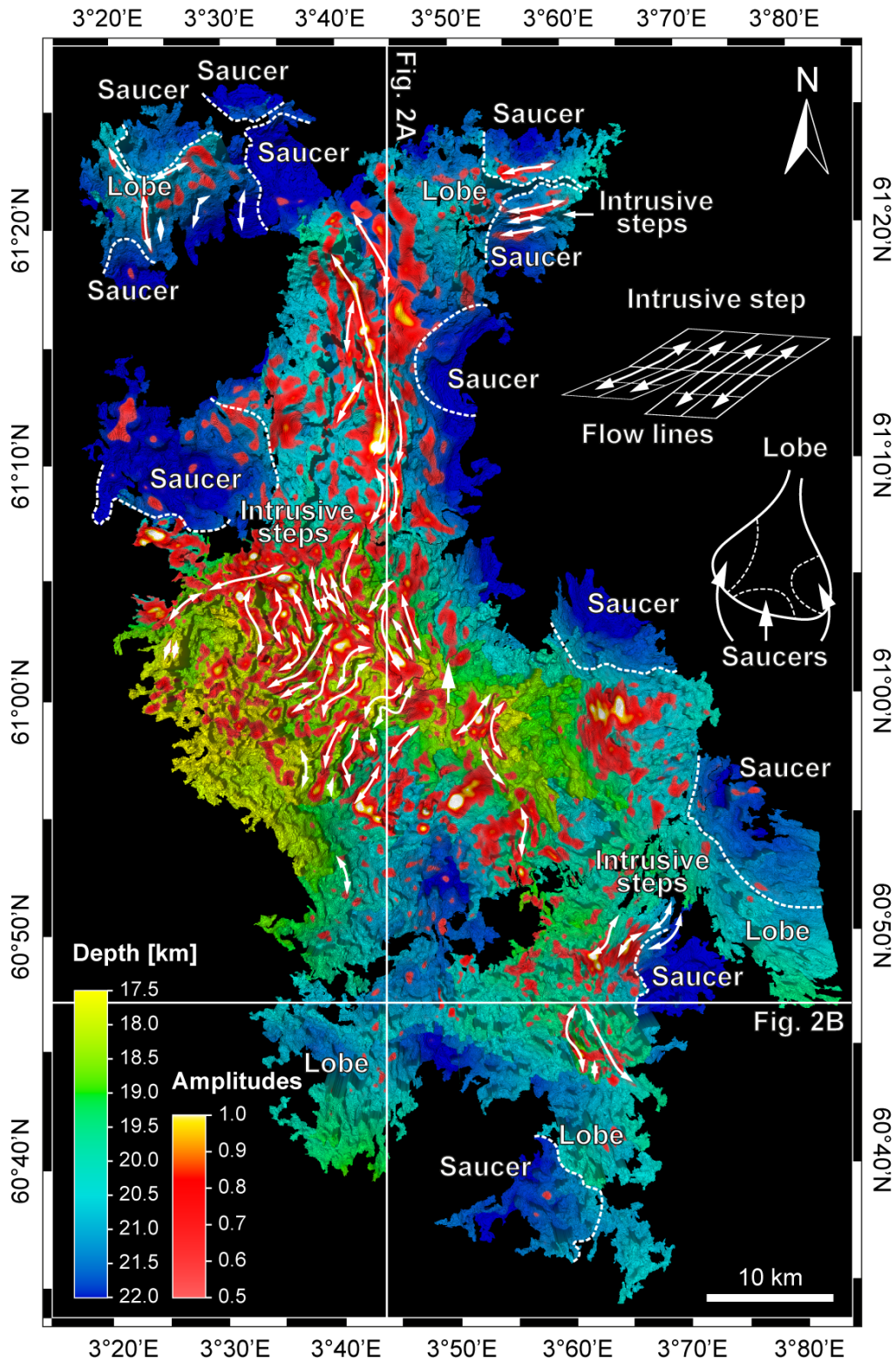
Figure 4: 3-D geometry of lower crustal reflection (LCR) originating from magmatic intrusions. Evidence for a magmatic intrusion includes: (1) significant lateral continuity ($\sim$2700 km^2); (2) irregular lobes extending outwards, (3) saucer-shape geometries; (4) intrusive steps and (5) elongated amplitude anomalies. Magma flow lines are drawn along amplitude anomalies and intrusive steps. Depth conversion is based on shallow (0-5 km) checkshot and deep (5-22 km) seismic data (Rosso, 2007; Bell et al., 2014). Seismic data courtesy of CGG.

6

Based on observed dominant frequencies of 10 ± 2 Hz (Fig. 2A) and seismic velocities of 6.9 ± 0.1 km/s for these basement rocks (values derived from a recent wide-angle 2-D seismic survey by Rosso (2007), we estimate that the LCR originates from a 180 ± 40 m thick body (Fig. 2C). This tuning thickness is consistent with an independent estimate based on an amplitude vs. thickness cross-plot (Connolly, 2005; Francis, 2015) (Fig. 2D) (see Appendix: Tuning thickness).

4 Discussion

In summary, we observe that the LCR shows typical effects of tuning (e.g. equal peak and trough amplitudes; Fig. 3E), which implies that it originates from a thin layer rather than the top of a several km-thick rock volume (see also Christiansson et al. (2000) and Fichler et al. (2011). In addition, the suggested eclogitization (Christiansson et al., 2000) and serpentinization origins for the LCR (Fichler et al., 2011) are at odds with observed velocities and the polarity of the LCR. For example, whilst eclogitization was initially postulated based on inferred seismic velocities of >8 km/s in the region of the LCR (Christiansson et al., 2000), recent wide-angle 2-D reflection and refraction data reveal normal velocities of 6.9 ± 0.1 km/s (Rosso, 2007) (see Appendix for more details). In contrast, serpentinization reduces seismic velocities (Christensen, 2004), which would result in a downward decrease in acoustic impedance and a negative polarity reflection, rather than the normal polarity we observe for the LCR (e.g. Figs. 2, 3I).

After examining previous interpretations of the LCR, we now discuss other explanations for lower crustal reflections. Reflections from highly strained rocks within a shear zone could explain the tuning effect, however shear zones are usually several kilometers thick in the lower crust and typically imaged as multiple, subparallel seismic reflections (Clerc et al., 2015; Fazlikhani et al., 2017). As such, it is difficult to explain the isolated reflection we observe (e.g. Fig. 2) in terms of a ductile, lower crustal shear zone. Instead, we observe that the LCR shows the characteristic features of magmatic intrusions observed in the field,

seismic reflection data, and numerical models (Fig. 3). First, the LCR crosscuts several inclined reflections (Fig. 3A). This pattern develops when magma cross-cuts existing stratigraphy without offsetting it (e.g. Cartwright and Hansen, 2006; Magee et al., 2016). Second, the LCR shows irregular lobes extending outward from the central axis (Fig. 3B); a feature commonly observed for magmatic intrusions in 3-D seismic reflection data (e.g. Smallwood and Maresh, 2002; Magee et al., 2016). Third, these lobes are themselves comprised of a series of saucers (Fig. 3C), a typical intrusion geometry observed in the field, seismic reflection data and numerical models (e.g. Polteau et al., 2008; Keller et al., 2013; Infante-Paez and Marfurt, 2018). Fourth, the LCR shows intrusive steps (Fig. 3D) formed during sheet propagation (e.g. Hansen et al., 2004; Magee et al., 2016; McBride et al., 2018). Fifth, the LCR shows typical tuning effects in the form of: (1) high amplitudes, (2) a peak-trough wavelet, and (3) approximately equal peak and trough amplitudes (e.g. Widess, 1973; Robertson and Nogami, 1984; Sheriff and Geldart, 1995) (Fig. 3E). Sixth, the LCR shows high amplitudes (Fig. 3F), which usually arise from the strong impedance contrast between magmatic intruded into sedimentary strata (e.g. Smallwood and Maresh, 2002). In the lower crust, where seismic velocities (6.9 ± 0.1 km/s; Rosso, 2007) are in the same range as those of magmatic rocks (~7 km/s; Smallwood and Maresh, 2002), high amplitudes are likely to arise from tuning of thin layers (Blundell, 1990). Seventh, these amplitudes occur in laterally, elongated anomalies (Fig. 3G); typical for magma flow patterns observed in 3-D seismic reflection data (e.g. Smallwood and Maresh, 2002). Eight, the LCR is continuous over a large area (~2700 km^2) (Fig. 3H), a typical feature of magmatic intrusions (e.g. Magee et al., 2016). Ninth, the LCR shows a positive polarity suggesting a positive impedance contrast typical for the top of an intrusion (Fig. 3I).

5 Implications

We estimate a magma volume of 472 ± 161 km^3 for the LCR by multiplying the surface area (~2700 km^2) with the inferred tuning thickness

(180±40 m). This estimate is of the same magnitude to the stacked lower crustal intrusions mapped in 2-D seismic reflection data from the North Atlantic margin (White et al., 2008; 540-600 km3) suggesting that the northern North Sea is more magmatic than previously thought.

We constrain the magma flow direction using intrusive steps (Fig. 3H) and amplitude anomalies (Fig. 3I) observed on the LCR (Fig. 4). Intrusive steps typically form parallel to the magma flow axis (see Magee et al., 2018 and references therein). The presence of up to 20 km long steps and amplitude anomalies, which may represent magma channels, within the LCR implies emplacement occurred primarily through lateral flow, rather than by amalgamation of many small sills each fed by a steep-to-vertical intrusion. Importantly, observed transgression of the LCR and evidence for extensive lateral flow suggests that magma flow in the lower crust, which is typically depicted as being dyke-dominated and with sills forming volumetrically minor storage reservoirs (e.g. Annen et al., 2005; Annen et al., 2015; Cashman et al., 2017; Edmonds et al., 2019), may also comprise a significant component of horizontal transport. While it is entirely possible that poorly imaged sub-seismic dikes did facilitate vertical magma transport to and upwards from the LCR, lateral transport clearly played a role in this and perhaps other cases. Integrating our understanding of how magma plumbing systems are constructed vertically and laterally is critical to resolving how magma moves through the crust, where it erupts, and how it impacts tectonic processes.

6 Conclusions

This study reveals a lower crustal magmatic intrusion in a continental rift (northern North Sea), which has long been considered magma-poor. The intrusion is ∼97 km long in North-South and ∼62 km wide in East-West direction showing evidence for significant lateral transport (up to 20 km) of large volumes of magma (472±161 km^3). This study highlights how advanced 3-D seismic imaging can help us understand the magmatic processes occurring deep within the crust.

Acknowledgements

References

Abdelmalak, M. M., Faleide, J. I., Planke, S., Gernigon, L., Zastrozhnov, D., Shephard, G. E., and Myklebust, R. (2017). The treflection and the deep crustal structure of the vring margin, offshore midnorway. *Tectonics*, 36(11):2497–2523.

Austrheim, H. (1987). Eclogitization of lower crustal granulites by fluid migration through shear zones. *Earth and Planetary Science Letters*, 81(2-3):221–232.

Bell, R. E., Jackson, C. A., Whipp, P. S., and Clements, B. (2014). Strain migration during multiphase extension: Observations from the northern north sea. *Tectonics*, 33(10):1936–1963.

Bingen, B., Nordgulen, O., and Viola, G. (2008). A four-phase model for the sveconorwegian orogeny, sw scandinavia. *Norwegian Journal of Geology*, 88(1):43–72.

Bingen, B. and Solli, A. (2009). Geochronology of magmatism in the caledonian and sveconorwegian belts of baltica: synopsis for detrital zircon provenance studies. *Norwegian Journal of Geology*, 89(4).

Blundell, D. (1990). Seismic images of continental lithosphere president's anniversary address 1989. *Journal of the Geological Society*, 147(6):895–913.

Brown, A. R. (2004). *Interpretation of three-dimensional seismic data*. The American Association of Petroleum Geologists and the Society of Exploration Geophysicists.

Cartwright, J. and Hansen, D. M. (2006). Magma transport through the crust via interconnected sill complexes. *Geology*, 34(11):929–932.

Christensen, N. I. (2004). Serpentinites, peridotites, and seismology. *International Geology Review*, 46(9):795–816.

Christiansson, P., Faleide, J., and Berge, A. (2000). Crustal structure in the northern north sea: an integrated geophysical study. *Geological Society, London, Special Publications*, 167(1):15–40.

Clerc, C., Jolivet, L., and Ringenbach, J.-C. (2015). Ductile extensional shear zones in the lower crust of a passive margin. *Earth and Planetary Science Letters*, 431:1–7.

Connolly, P. (2005). Net pay estimation from seismic attributes. In *67th EAGE Conference & Exhibition*.

Fazlikhani, H., Fossen, H., Gawthorpe, R. L., Faleide, J. I., and Bell, R. E. (2017). Basement structure and its influence on the structural configuration of the northern north sea rift. *Tectonics*, 36(6):1151–1177.

Fichler, C., Odinsen, T., Ruesltten, H., Olesen, O., Vindstad, J. E., and Wienecke, S. (2011). Crustal inhomogeneities in the northern north sea from potential field modeling: Inherited structure and serpentinites? *Tectonophysics*, 510(1):172–185.

Fossen, H. and Dunlap, W. J. (1999). On the age and tectonic significance of permo-triassic dikes in the bergen-sunnhordland region, southwestern norway. *Norsk Geologisk Tidsskrift*, 79(3):169–177.

Francis, A. (2015). A simple guide to seismic amplitudes and detuning. *GEO ExPro*.

Hansen, D. M., Cartwright, J. A., and Thomas, D. (2004). 3d seismic analysis of the geometry of igneous sills and sill junction relationships. *Geological Society, London, Memoirs*, 29(1):199–208.

Heeremans, M. and Faleide, J. I. (2004). Late carboniferous-permian tectonics and magmatic activity in the skagerrak, kattegat and the north sea. *Geological Society, London, Special Publications*, 223(1):157–176.

Huismans, R. and Beaumont, C. (2011). Depth-dependent extension, two-stage breakup and cratonic underplating at rifted margins. *Nature*, 473(7345):74–78.

Infante-Paez, L. and Marfurt, K. J. (2018). In-context interpretation: Avoiding pitfalls in misidentification of igneous bodies in seismic data. *Interpretation*, 6(4):SL29–SL42.

Keller, T., May, D. A., and Kaus, B. J. (2013). Numerical modelling of magma dynamics coupled to tectonic deformation of lithosphere and crust. *Geophysical Journal International*, 195(3):1406–1442.

Magee, C., Muirhead, J., Schofield, N., Walker, R. J., Galland, O., Holford, S., Spacapan, J., Jackson, C. A., and McCarthy, W. (2018). Structural signatures of igneous sheet intrusion propagation. *Journal of Structural Geology*.

Magee, C., Muirhead, J. D., Karvelas, A., Holford, S. P., Jackson, C. A. L., Bastow, I. D., Schofield, N., Stevenson, C. T. E., McLean, C., McCarthy, W., and Shtukert, O. (2016). Lateral magma flow in mafic sill complexes. *Geosphere*, 12(3):809–841.

Maystrenko, Y. P., Olesen, O., Ebbing, J., and Nasuti, A. (2017). Deep structure of the northern north sea and southwestern norway based on 3d density and magnetic modelling. *Norwegian Journal of Geology/Norsk Geologisk Forening*, 97(3).

McBride, J. H., William Keach, R., Leetaru, H. E., and Smith, K. M. (2018). Visualizing precambrian basement tectonics beneath a carbon capture and storage site, illinois basin. *Interpretation*, 6(2):T257–T270.

Odinsen, T., Christiansson, P., Gabrielsen, R. H., Faleide, J. I., and Berge, A. M. (2000). The geometries and deep structure of the northern north sea rift system. *Geological Society, London, Special Publications*, 167(1):41–57.

Planke, S., Rasmussen, T., Rey, S., and Myklebust, R. (2005). Seismic characteristics and distribution of volcanic intrusions and hydrothermal vent complexes in the vring and mre basins. *Petroleum Geology Conference series*, 6:833–844.

Polteau, S., Mazzini, A., Galland, O., Planke, S., and Malthe-Srenssen, A. (2008). Saucer-shaped intrusions: Occurrences, emplacement and implications. *Earth and Planetary Science Letters*, 266(1):195–204.

Robertson, J. D. and Nogami, H. H. (1984). Complex seismic trace analysis of thin beds. *Geophysics*, 49(4):344–352.

Rosso, A. (2007). *Deep crustal geometry: An integrated geophysical study of an exhumed eclogite terrain, Bergen Area, Southwest Norway.* Thesis, The Graduate School of the University of Wyoming.

Sheriff, R. E. and Geldart, L. P. (1995). *Exploration Seismology.* Cambridge University Press.

Smallwood, J. R. and Maresh, J. (2002). The properties, morphology and distribution of igneous sills: modelling, borehole data and 3d seismic from the faroe-shetland area. *Geological Society, London, Special Publications*, 197(1):271–306.

Torsvik, T. H., Smethurst, M. A., Burke, K., and Steinberger, B. (2008). Long term stability in deep mantle structure: Evidence from the 300 ma skagerrak-centered large igneous province (the sclip). *Earth and Planetary Science Letters*, 267(3-4):444–452.

Trude, J., Cartwright, J., Davies, R. J., and Smallwood, J. (2003). New technique for dating igneous sills. *Geology*, 31(9):813–816.

Weatherall, P., Marks, K., Jakobsson, M., Schmitt, T., Tani, S., Arndt, J. E., Rovere, M., Chayes, D., Ferrini, V., and Wigley, R. (2015). A new digital bathymetric model of the world's oceans. *Earth and Space Science*, 2(8):331–345.

White, R., Smith, L., Roberts, A., Christie, P., Kusznir, N., Roberts, A., Healy, D., Spitzer, R., Chappell, A., and Eccles, J. (2008). Lower-crustal intrusion on the north atlantic continental margin. *Nature*, 452(7186):460–464.

Widess, M. (1973). How thin is a thin bed? *Geophysics*, 38(6):1176–1180.

Appendix

Seismic acquisition: The seismic data (courtesy of CGG) were acquired with a G-Gun array consisting of 3 subarrays with a source array depth of 6-9 m; a source length of 16-18 m; a SP interval of 18.75 m; source separation of 37.5 m; a volume of 4550 in^3 and an air pressure of 2000 psi. The streamer consisted of 12 up to 8 km long cables with 636 channels each; a cable separation of 75 m and group spacing of 12.5 m; depths of 7-50 m covering offsets of 150-8100 m. The data was recorded with a 2 ms sample interval; 9000 ms recording length; a low cut filter (2Hz-6db/oct) and high cut (200 Hz-370 db/oct) filter.

Seismic processing: The seismic data were processed in 90 steps including: divergence compensation; low cut filter (1.5 Hz, 2.5 Hz); noise attenuation (e.g. swell, direct wave); spatial anti-aliasing filter (12.5 m group interval); direct wave attenuation; source de-signature; de-spike; time-variant high cut filter; receiver motion correction and de-ghosting; FK filter; cold water and tidal statics; multiple modelling with adaptive subtraction; Tau-P mute; Radon de-multiple; far angle destriping; multiple attenuation; binning (75 m interval, 107 offset planes); acquisition hole infill; 5-D regularization; 3-D true amplitude Kirchhoff pre-stack time migration; residual move-out correction; Linear FL Radon; full offset stack with time-variant inner and out mute; acquisition footprint removal; crossline K filter; residual destriping and dynamic Q-compensation. The seismic volume was zero phase processed with SEG normal polarity.

Lower crustal velocities: Christiansson et al. (2000) show 1-D velocity-depth functions derived from two-ship seismic refraction data at two locations (ESP 50, ESP 51) with different methods (slope-intercept, Herglotz-Wiecherts, t^2-x^2, tau-p, forward model). At ESP 50, the slope intercept and tau-p method indicate lower crustal velocities of 8 km/s. At ESP 51, the slope intercept, t^2-x^2 and forward model suggest lower crustal velocities of 8 km/s. All other methods provide no velocity estimate for the lower crust. Odinsen et al. (2000) and Fichler et al. (2011) do not derive new velocity-depth data.

Rosso (2007) derives new 2-D velocity-depth data by combining reflection and refraction data recorded along two transects (8 OBS and 8 REFTEK receivers) with Transect 1 (NSDP84-1) passing the two locations (ESP 50, ESP 51) analyzed by Christiansson et al. (2000). Based on a comprehensive analysis including event picking, ray-tracing and uncertainty estimation for the entire dataset, Rosso (2007) conclude that the lower crust has velocities of 6.9±0.1 km/s.

Tuning thickness: While we have already estimated the tuning thickness (180±40 m) from the seismic velocity (6.9±0.1 km/s) and dominant frequency (10±2 Hz) of the interval of interest as a quarter of the wavelength ($\lambda/4=v/f/4$), we validate this value with a second estimate based on the amplitude versus thickness cross-plot (Fig. 2D). This estimate is based on the effect that an amplitude maximum occurs at the point of maximum constructive interference between the top and base reflection, i.e. the tuning thickness (Connolly, 2005; Francis, 2015). For this estimate, we first extract the amplitude of the top of the LCR and then calculate the thickness by multiplying the time difference between top and base of the LCR with the seismic velocity (6.9±0.1 km/s; Rosso, 2007). Cross-plotting the amplitude versus thickness reveals a maximum at a thickness of ∼180 m indicating that this tuning thickness estimate is consistent with the standard estimate based on a quarter of the wavelength.

Supplementary Figures
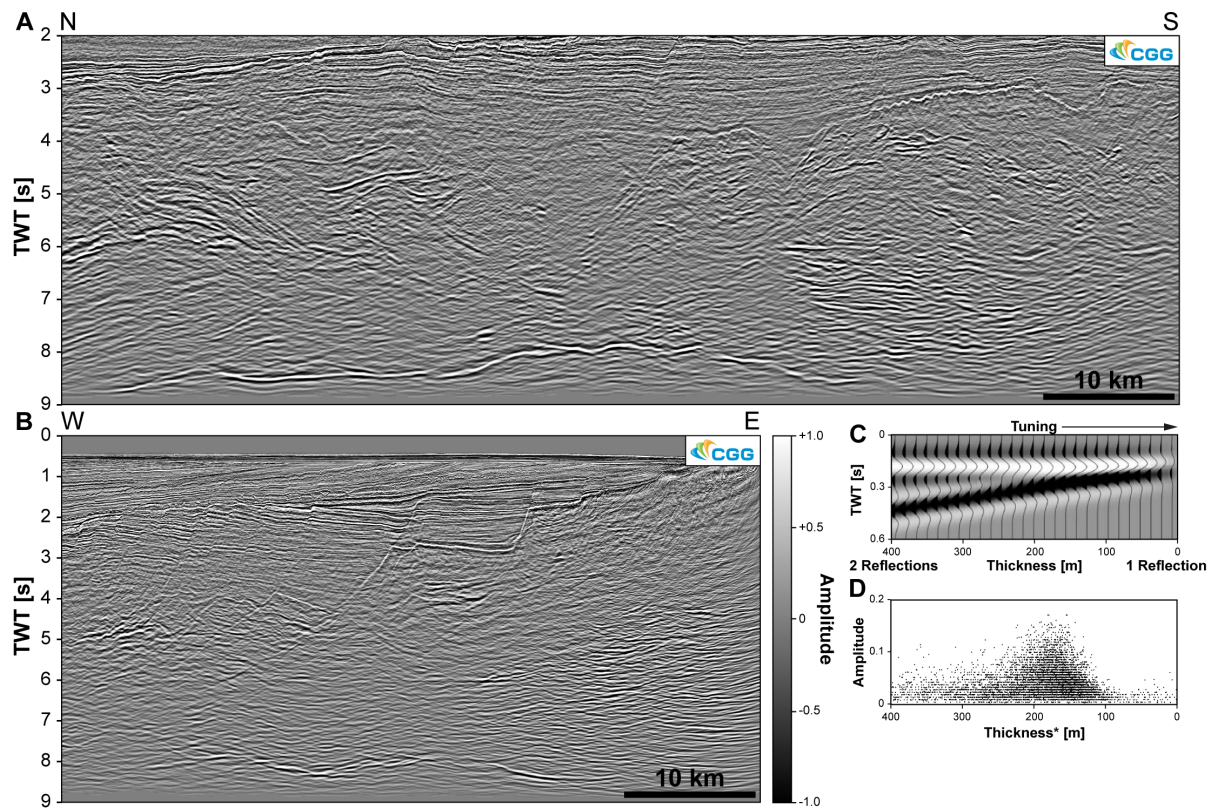
Supp. Figure 1: Uninterpreted version of Figure 2.
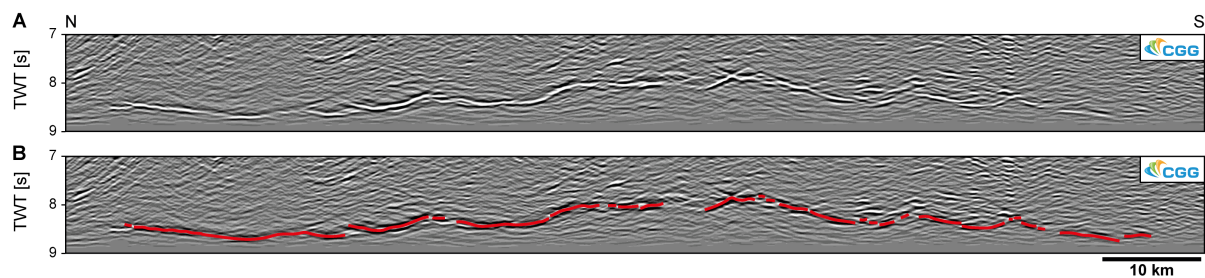
Supp. Figure 2: **A** Uninterpreted and **B** interpreted seismic section equivalent to Figure 3H.